crystals

MDPI

Article

$Lu_5Pd_4Ge_8$ and $Lu_3Pd_4Ge_4$: Two More Germanides among Polar Intermetallics

Riccardo Freccero [1], Pavlo Solokha [1,*], Davide Maria Proserpio [2,3], Adriana Saccone [1] and Serena De Negri [1]

1 Dipartimento di Chimica e Chimica Industriale, Università degli Studi di Genova, Via Dodecaneso 31, 16146 Genova, Italy; riccardo.freccero@edu.unige.it (R.F.); adriana.saccone@unige.it (A.S.); serena.denegri@unige.it (S.D.N.)

2 Dipartimento di Chimica, Università degli Studi di Milano, Via Golgi 19, 20133 Milano, Italy; davide.proserpio@unimi.it

3 Samara Center for Theoretical Materials Science (SCTMS), Samara State Technical University, Molodogvardeyskaya St. 244, Samara 443100, Russia

* Correspondence: pavlo.solokha@unige.it; Tel.: +39-010-3536-159

Received: 20 April 2018; Accepted: 3 May 2018; Published: 5 May 2018

Abstract: In this study, two novel $Lu_5Pd_4Ge_8$ and $Lu_3Pd_4Ge_4$ polar intermetallics were prepared by direct synthesis of pure constituents. Their crystal structures were determined by single crystal X-ray diffraction analysis: $Lu_5Pd_4Ge_8$ is monoclinic, $P2_1/m$, $mP34$, a = 5.7406(3), b = 13.7087(7), c = 8.3423(4) Å, β = 107.8(1), Z = 2; $Lu_3Pd_4Ge_4$ is orthorhombic, $Immm$, $oI22$, a = 4.1368(3), b = 6.9192(5), c = 13.8229(9) Å, Z = 2. The $Lu_5Pd_4Ge_8$ analysed crystal is one more example of non-merohedral twinning among the rare earth containing germanides. Chemical bonding DFT studies were conducted for these polar intermetallics with a metallic-like behavior. Gathered results for $Lu_5Pd_4Ge_8$ and $Lu_3Pd_4Ge_4$ permit to described both of them as composed by $[Pd–Ge]^{\delta-}$ three dimensional networks bonded to positively charged lutetium species. From the structural chemical point of view, the studied compounds manifest some similarities to the Zintl phases, containing well-known covalent fragments i.e., Ge dumbbells as well as unique *cis*-Ge_4 units. A comparative analysis of molecular orbital diagrams for Ge_2^{6-} and *cis*-Ge^{10-} anions with COHP results supports the idea of the existence of complex Pd–Ge polyanions hosting covalently bonded partially polarised Ge units. The palladium atoms have an anion like behaviour and being the most electronegative cause the noticeable variation of Ge species charges from site to site. Lutetium charges oscillate around +1.5 for all crystallographic positions. Obtained results explained why the classical Zintl-Klemm concept can't be applied for the studied polar intermetallics.

Keywords: polar intermetallics; symmetry reduction; chemical bond

1. Introduction

In *RE*–Pd–Ge systems (*RE* = rare earth metal) more than one hundred ternary compounds have already been discovered [1], which have been extensively studied with respect to crystal structure, chemical bonding and physical properties [2–6].

The structures of Ge-rich compounds are characterized by a variety of Ge covalent fragments, with topologies depending both on global stoichiometry and on the nature of the *RE* component. These units are often joined together through Pd atoms, meanwhile the *RE* species are located in bigger channels inside the structure [2,3,7]. The frameworks formed by Pd and Ge atoms have been interpreted as polyanions of general formula $[Pd_xGe_y]^{\delta-}$ counterbalanced by the rare earth cations, coherently with the definition of these compounds as polar intermetallics [4].

It is interesting to remark that the ternary *RE*–Pd–Ge compounds manifest a tendency to be stoichiometric with ordered distributions of constituents through distinct Wyckoff sites. Moreover, within Pd–Ge fragments, both species have small coordination numbers (usually four or five) with very similar topological distributions of neighbours (tetrahedral coordination or its derivatives). These features may be considered as geometrical traces of a similar chemical role of Pd and Ge. That is why symmetry reduction from certain aristotypes can conveniently depict the distortions related with an ordered distribution of atom sorts. Such analysis has been conducted in the literature for AlB_2 derivative polymorphs of *RE*PdGe [8] and $BaAl_4$ derivatives of the $RE_2Pd_3Ge_5$ [7,9] family of compounds. In systems where such types of relationships exist, the geometric factor is surely of great importance. Thus, varying *RE*, different polymorphs [8] or even novel compounds may form. As an example, heavy rare earth containing $RE_5Pd_4Ge_8$ (*RE* = Er, Tm) [4] and $RE_3Pd_4Ge_4$ (*RE* = Ho, Tm, Yb) [3] series of compounds may be cited.

During exploratory syntheses conducted in the Lu–Pd–Ge system in the framework of our ongoing studies on Ge-rich ternary compounds, the Lu representatives of the abovementioned 5:4:8 and 3:4:4 stoichiometries were detected for the first time. In this paper, results on the synthesis and structural characterization/analysis of these new germanides are reported, together with an extensive study of their chemical bonding, including Bader charges, Density of States (DOS) and Crystal Orbital Hamilton Population (COHP) curves as well as Molecular Orbitals (MO) diagrams for Zintl anions composed by Ge.

2. Experimental

2.1. Synthesis and SEM-EDXS Characterization

The Lu–Pd–Ge alloys were synthesized from elements with nominal purities >99.9% mass. Lutetium was supplied by Newmet Koch, Waltham Abbey, England, and palladium and germanium by MaTecK, Jülich, Germany.

Different synthetic routes were followed, including arc melting and direct synthesis in resistance furnace. In the latter case, proper amounts of components were placed in an alumina crucible, which was closed in an evacuated quartz ampoule to prevent oxidation at high temperatures, and submitted to one of the following thermal cycles in a resistance furnace:

(1) 25 °C → (10 °C/min) → 950 °C (1 h) → (−0.2 °C/min) → 600 °C (168 h) → (−0.5 °C/min) → 300 °C → furnace switched off

(2) 25 °C → (10 °C/min) → 1150 °C (1 h) → (−0.2 °C/min) → 300 °C → furnace switched off

A continuous rotation of the quartz ampoule during the thermal cycle was applied. In some cases, the thermal treatment followed arc melting. A scanning electron microscope (SEM) Zeiss Evo 40 (Carl Zeiss SMT Ltd., Cambridge, UK) coupled with a Pentafet Link Energy Dispersive X-ray Spectroscopy (EDXS) system managed by INCA Energy software (Oxford Instruments, Analytical Ltd., Bucks, UK) was used for microstructure observation and phase analysis. For this last purpose, calibration was performed with a cobalt standard. Samples to be analyzed were embedded in a phenolic resin with carbon filler, by using the automatic hot compression mounting press, Opal 410 (ATM GmbH, Mammelzen, Germany), and smooth surfaces for microscopic examinations were obtained with the aid of the automatic grinding and polishing machine, Saphir 520 (ATM GmbH, Mammelzen, Germany). SiC papers with grain sizes decreasing from 600 to 1200 mesh and diamond pastes with particle sizes decreasing from 6 to 1 μm were employed for grinding and polishing, respectively.

2.2. X-ray Diffraction (XRD) Measurements on Single Crystals and Powder Samples

Single crystals of $Lu_5Pd_4Ge_8$ and $Lu_3Pd_4Ge_4$ were selected from suitable samples with the aid of a light optical microscope operated in dark field mode. A full-sphere dataset was obtained in a routine fashion at ambient conditions on a four-circle Bruker Kappa APEXII CCD area-detector diffractometer

equipped by the graphite monochromatized Mo $K\alpha$ (λ = 0.71073 Å) radiation, operating in ω-scan mode. Crystals exhibiting metallic luster and glued on glass fibers were mounted in a goniometric head and then placed in a goniostat inside a diffractometer camera. Intensity data were collected over the reciprocal space up to ~30° in θ with exposures of 20 s per frame. Semi-empirical absorption corrections based on a multipolar spherical harmonic expansion of equivalent intensities were applied to all data by the SADABS/TWINABS (2008) software [10].

The corresponding CIF files are available in the supporting information material and they have also been deposited at Fachinformationszentrum Karlsruhe, 76344 Eggenstein-Leopoldshafen, Germany, with the following depository numbers: CSD-434226 ($Lu_5Pd_4Ge_8$) and CSD-434225 ($Lu_3Pd_4Ge_4$). Selected crystallographic data and structure refinement parameters for the studied single crystals are listed in Table 1. Details regarding the structure solution are discussed in Section 3.2. X-ray powder diffraction (XRPD) measurements were performed on all samples, using a Philips *X'Pert* MPD vertical diffractometer (Cu $K\alpha$ radiation, λ = 1.5406 Å, graphite crystal monochromator, scintillation detector, step mode of scanning). Phase identification was performed with the help of the PowderCell software, version 2.4 [11].

Table 1. Crystallographic data for $Lu_5Pd_4Ge_8$ and $Lu_3Pd_4Ge_4$ single crystals together with some experimental details of their structure determination.

Empirical Formula	**$Lu_5Pd_4Ge_8$**	**$Lu_3Pd_4Ge_4$**
EDXS data	$Lu_{28.6}Pd_{24.9}Ge_{46.5}$	$Lu_{25.7}Pd_{35.0}Ge_{39.5}$
Space group (No.)	$P2_1/m$ (11)	*Immm* (71)
Pearson symbol-prototype, Z	$mP34$-$Tm_5Pd_4Ge_8$, 2	$oI22$-$Gd_3Cu_4Ge_4$, 2
a [Å]	5.7406(3)	4.1368(3)
b [Å]	13.7087(7)	6.9192(5)
c [Å]	8.3423(4)	13.8229(9)
β (°)	107.8(1)	–
V [Å^3]	625.20(5)	395.66(5)
Abs. coeff. (μ), mm^{-1}	63.5	60.7
Twin law	$[-\frac{1}{2}\ 0\ \frac{1}{2}; 0\ -1\ 0;\ \frac{3}{2}\ 0\ \frac{1}{2}]$	–
k (BASF)	0.49(1)	–
Unique reflections	2105	404
Reflections I > 2σ(I)/parameters	1877/87	398/23
GOF on F^2 (S)	1.17	1.17
R indices [I > 2σ(I)]	R1 = 0.0190;wR2 = 0.0371	R1 = 0.0238;wR2 = 0.0869
R indices [all data]	R1 = 0.0247;wR2 = 0.0384	R1 = 0.0242;wR2 = 0.0871
$\Delta\varrho_{fin}$ (max/min), [e/Å^3]	2.00/−2.83	2.87/−3.33

2.3. Computational Details

A charge analysis based on Bader's Quantum Theory of Atoms In Molecules (QTAIM) [12], coded in the Vienna Ab-initio Simulation Package (VASP) [13], was used to evaluate the atomic charge populations in the title compounds. Projector augmented waves (PAW) formalism was used, together with Perdew–Berke–Erzenhof parametrization of the exchange-correlation interaction. The recommended PAW sets were used, considering nine valence electrons for Lu ($6s^25p^65d^1$), ten for Pd ($5s^14d^9$), and fourteen for Ge ($4s^23d^{10}4p^2$). An energy cut-off of 600 eV was set for all calculations presented and the default value (10^{-5} eV) of the energy convergence was used.

The electronic band structures of $Lu_5Pd_4Ge_8$ and $Lu_3Pd_4Ge_4$ were calculated by means of the self-consistent, tight-binding, linear-muffin-tin-orbital, atomic-spheres approximation method using the Stuttgart TB-LMTO-ASA 4.7 program [14], within the local density approximation (LDA) [15] of DFT. The radii of the Wigner–Seitz spheres were assigned automatically so that the overlapping potentials would be the best possible approximations to the full potential, and no empty spheres were needed to meet the minimum overlapping criterion.

The basis sets included 6*s*/(6*p*)/5*d* orbitals for Lu with Lu $4f^{14}$ treated as core, 5*s*/5*p*/4*d*/(4*f*) for palladium and 4*s*/4*p*/(4*d*)/(4*f*) orbitals for germanium with orbitals in parentheses being downfolded.

The Brillouin zone integrations were performed by an improved tetrahedron method using a 20 × 8 × 12 *k*-mesh for $Lu_5Pd_4Ge_8$ and 16 × 16 × 16 for $Lu_3Pd_4Ge_4$.

Crystal Orbital Hamilton populations (COHPs) [16] were used to analyze chemical bonding. The integrated COHP values (*i*COHPs) were calculated in order to evaluate the strengths of different interactions. Plots of DOS and COHP curves were generated using wxDragon [17], setting the Fermi energy at 0 eV as a reference point.

Qualitative MO arguments based on extended Hückel theory (EHT) have been developed with the CACAO package [18,19] and its graphic interface. Even if the EHT model tends to involve the most drastic approximations in MO theory, this one electron effective Hamiltonian method tends to be used to generate qualitatively correct molecular and crystal orbitals [20]. EHT is best used to provide models for understanding both molecular and solid state chemistry, as shown with great success by Roald Hoffmann and others [21].

3. Results and Discussion

3.1. Results of SEM-EDXS Characterization

An explorative study of the Ge-rich region of the Lu–Pd–Ge system was conducted by synthesis of some ternary samples with a Ge content >40 at %. The prepared samples are listed in Table 2, together with an indication of the followed synthetic route, as well as the results of SEM/EDXS characterization. Information on phase crystal structure was obtained from X-ray diffraction results.

Table 2. Results of SEM/EDXS characterization of the Lu–Pd–Ge samples (> 40 at % Ge) obtained with different synthesis methods/thermal treatments. The highest yield phase in each sample is the first in the list.

No. Overall Composition [at %] Synthesis/Thermal Treatment	Phases	Phase Composition [at %] Lu; Pd; Ge	Crystal Structure
1 $Lu_{21.4}Pd_{11.2}Ge_{67.4}$ Arc melting followed by thermal treatment (1)	Lu_2PdGe_6 $Lu_5Pd_4Ge_8$ $LuPd_{0.16}Ge_2$ Ge	21.5; 12.1; 66.4 28.6; 25.1; 46.3 31.1; 5.4; 63.5 –; –; –;	*oS*72–$Ce_2(Ga_{0.1}Ge_{0.9})_7$ *mP*34-$Tm_5Pd_4Ge_8$ *oS*16-$CeNiSi_2$ *cF*8-C
2 $Lu_{28.9}Pd_{24.1}Ge_{47.0}$ Arc melting	$Lu_5Pd_4Ge_8$ new phase Lu_2PdGe_6 $LuPd_{0.16}Ge_2$	28.8; 24.8; 46.4 32.4; 28.5; 39.1 21.7; 11.8; 66.5 30.1; 6.9; 63.0	*mP*34-$Tm_5Pd_4Ge_8$ AlB_2 related *oS*72–$Ce_2(Ga_{0.1}Ge_{0.9})_7$ *oS*16-$CeNiSi_2$
3 * $Lu_{30.8}Pd_{25.5}Ge_{43.7}$ Direct synthesis with thermal treatment (2)	$Lu_5Pd_4Ge_8$ new phase Ge	28.6; 24.9; 46.5 33.0; 26.8; 40.2 –; –; –;	*mP*34-$Tm_5Pd_4Ge_8$ AlB_2 related *cF*8-C
4 * $Lu_{33.0}Pd_{26.0}Ge_{41.0}$ Arc melting followed by thermal treatment (2)	$Lu_3Pd_4Ge_4$ $Lu_5Pd_4Ge_8$ LuPdGe PdGe Ge	25.7; 35.0; 39.5 28.4; 25.1; 46.5 31.9; 34.5; 33.6 0.0; 53.4; 47.6 0.0; 0.0; 100.0	*oI*22-$Gd_3Cu_4Ge_4$ *mP*34-$Tm_5Pd_4Ge_8$ *oI*36-AuYbSn *oP*8-FeAs *cF*8-C
5 $Lu_{17.9}Pd_{29.0}Ge_{53.1}$ Arc melting	$Lu_3Pd_4Ge_4$ LuPdGe PdGe Ge	26.1; 34.2; 39.7 32.0; 33.5; 34.5 0.0; 52.4; 47.8 0.0; 0.0; 100.0	*oI*22-$Gd_3Cu_4Ge_4$ *oI*36-AuYbSn *oP*8-FeAs *cF*8-C

* Samples from which single crystals were taken.

All samples are multiphase, as it is common for non-annealed alloys belonging to complex ternary systems, Ge is always present, in some cases in small amount. SEM images using the Back-Scattered Electron (BSE) mode are well contrasted, helping to distinguish different compounds, whose compositions are highly reproducible.

Several ternary compounds already known from the literature were detected in the samples, namely Lu_2PdGe_6, $LuPd_{0.16}Ge_2$ and LuPdGe [1,2]. For the latter, the *oI*36-AuYbSn structure was confirmed, in agreement with previous single crystal data [8].

A new phase of composition ~$Lu_{33}Pd_{27}Ge_{40}$ was detected in samples 2 and 3; the corresponding X-ray powder patterns could be acceptably indexed assuming a simple AlB_2-like structure, with a ≈ 4.28 and c ≈ 3.54 Å. Nevertheless, a deeper structural investigation would be necessary to ensure its crystal structure.

Crystal structures of the new $Lu_5Pd_4Ge_8$ and $Lu_3Pd_4Ge_4$ compounds were solved by analysing single crystals extracted from samples 3 and 4, respectively. The obtained structural models, discussed in the following section, were consistent with the measured powder patterns.

3.2. Crystal Structures of $Lu_5Pd_4Ge_8$ and $Lu_3Pd_4Ge_4$

3.2.1. Structural Determination

The $Lu_5Pd_4Ge_8$ crystal selected for X-ray analysis is one more example of non-merohedral twins among germanides. Previously, similar twins were found for Tb_3Ge_5 [22], Eu_3Ge_5 [23], Pr_4Ge_7 [24], La_2PdGe_6 and Pr_2PdGe_6 [2]. Based on the preliminary indexing results, the unit cell of the measured crystal might be considered as a base centered orthorhombic one with a = 8.55, b = 21.29 and c = 13.70 Å. The analysis of systematic extinctions suggested the following space groups: $Cmc2_1$ (No. 36), $C2cm$ (No. 40) and $Cmcm$ (No. 63). It should be mentioned that the average value of $|E^2-1|$ = 1.33, characterizing the distribution of peak intensities, deviates noticeably from the ideal value (0.968) for centrosymmetric space groups. Frequently, this is an indication of a twinned dataset [25,26]. A charge-flipping algorithm implemented in JANA2006 [27] was used, giving a preliminary structural model with 36 Lu atoms and 96 Ge atoms in the unit cell (*Cmcm* space group). Usually, when scatterers have such remarkable differences in electrons, the charge-flipping algorithm is quick and very efficient in discriminating them. Considering the interatomic distances criterion and U_{eq} values, in the successive iteration cycles, Pd atoms were introduced manually by substituting those of Ge, but no improvements were observed. There was no chance to improve this model further because the isotropic thermal displacement parameters showed meaningless values; several additional strong peaks were present at difference Fourier maps located too close to the accepted atom positions; and the R1 value stuck at ca. 10%. Looking for a correct structure solution in other space groups gave no reasonable results.

At this point, a more careful analysis of diffraction spots in reciprocal space was performed using RLATT [10] software. It was noticed that a remarkable number of peaks distributed in a regular way had a small intensity and might be considered as super reflections. Therefore, they were ignored during the indexing procedure, and a four times smaller primitive monoclinic unit cell with a = 5.73, b= 13.70, c = 8.34 Å and β = 107.8° was derived. The dataset was newly integrated and semi-empirical absorption corrections were applied by SADABS [10] software. This time, an *mP*34 structural model, containing all the atomic species, was proposed by the charge-flipping algorithm. Even so, the refinement was not satisfactory because some Wyckoff sites manifested partial occupancy and it was not possible to refine the structure anisotropically. It was decided to test the ROTAX [28] algorithm implemented in WinGx [29] and check the possibility of interpreting our crystal as a non-merohedral twin. In fact, a two-fold rotation along the [101] direction $\begin{pmatrix} \frac{-1}{2} & 0 & \frac{1}{2} \\ 0 & -1 & 0 \\ \frac{3}{2} & 0 & \frac{1}{2} \end{pmatrix}$ was proposed as a twin law obtaining a good figure of merit.

To check this hypothesis and refine the collected data as accurately as possible, the initially selected batch of ca. 1000 reflections (comprising those of weak intensity considered as super reflections) was separated into two groups with the help of the CELL_NOW [10] program, suggesting the same twin law for the two monoclinic domains. Successively, the information on the reciprocal domain orientation stored in the .p4p file was used to integrate the dataset considering the simultaneous presence of both domains. After that, the resulting intensities set was scaled, corrected for absorption and merged with the help of the TWINABS [10] program. As a result, the output in HKLF5 format with a flag indicating the original domains, was generated. Using the latter and testing one more time the charge flipping procedure, the structural model was immediately found and element species were correctly assigned. The $Lu_5Pd_4Ge_8$ was of monoclinic symmetry (space group $P2_1/m$, $mP34$-$Tm_5Pd_4Ge_8$) and contained 3 Lu, 2 Pd and 6 Ge crystallographic sites. All the atom positions were completely occupied and did not manifest any considerable amount of statistical mixture. The anisotropically refined $Lu_5Pd_4Ge_8$ showed excellent residuals and flat difference Fourier maps (see Table 1). The refined volume ratio of twinned domains was 0.49/0.51.

The RLATT program was used to generate a picture showing the distribution of X-ray diffraction spots originating from the two domains, differentiated by color, in Figure 1 (upper part). The distribution of the non-overlapped peaks of the second domain was also easily visible on the precession photo of the *h*3*l* zone, demonstrated in Figure 1 (lower part). In the same figure, a schematic real space representation of the mutual orientation of the twinned-crystal components is shown.

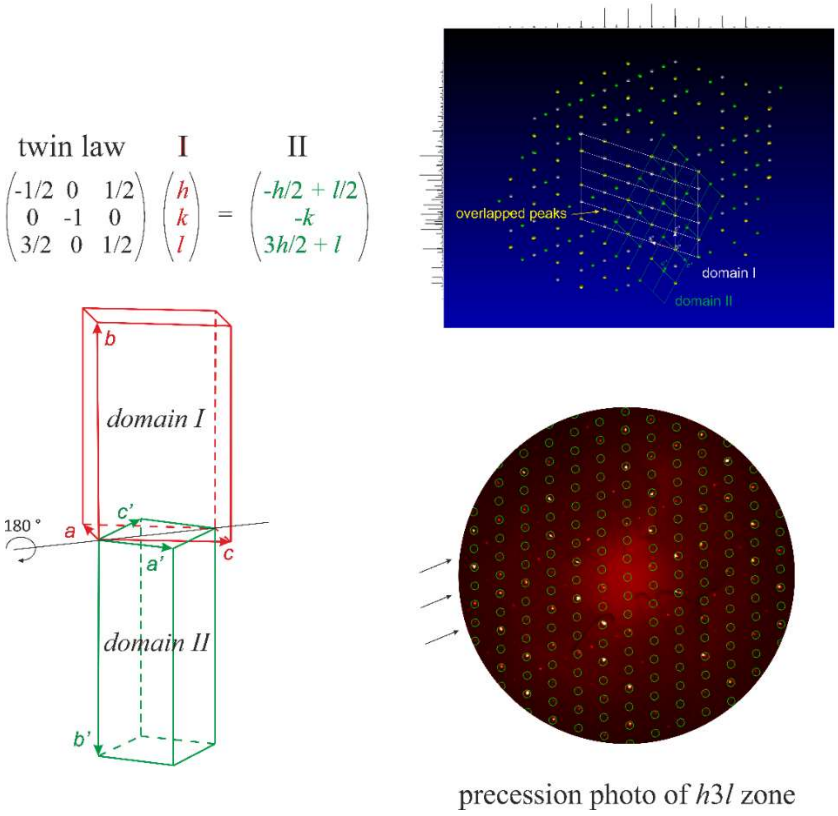

Figure 1. Twin law and reciprocal orientation of the two domains in the $Lu_5Pd_4Ge_8$ twinned crystal (**left**); distribution of the diffraction peaks in the reciprocal space (**right**). Nodes of the reciprocal pattern for each domain are shown in white and green, and overlapped peaks are yellow. On the experimental precession photos of the *h*3*l* zone, arrows indicate the directions along which the second domain peaks are easily visible.

Indexing of the diffraction dataset of the $Lu_3Pd_4Ge_4$ single crystal gave an orthorhombic base centered unit cell with a = 4.137, b = 6.919, c = 13.823 Å. Systematic extinction conditions related to the presence of symmetry elements were not found for this dataset. The structure solution was found in *Immm* with the aid of the charge flipping algorithm implemented in JANA2006 [27]. The proposed preliminary structural model contained five crystallographic sites, giving the $Lu_3Pd_4Ge_4$ formula and corresponding to the *oI*22-$Gd_3Cu_4Ge_4$ prototype. Partial site occupation (due to a possible statistical mixture of the species) was checked in separate cycles of least-squares refinement, but no significant deviation from full occupation was detected. The final structure model was refined as stoichiometric with the anisotropic displacement parameters for all crystallographic sites, giving small residual factors and a flat difference Fourier map (see Table 1). The standardized atomic coordinates for $Lu_5Pd_4Ge_8$ and $Lu_3Pd_4Ge_4$ are given in Table 3.

Table 3. Atomic coordinates standardized by Structure Tidy [30] and equivalent isotropic displacement parameters for $Lu_5Pd_4Ge_8$ and $Lu_3Pd_4Ge_4$.

Atom	Site	*x*/*a*	*y*/*b*	*z*/*c*	U_{eq} (Å^2)
			$Lu_5Pd_4Ge_8$		
Lu1	2*e*	0.71858(8)	1/4	0.93028(6)	0.0047(1)
Lu2	4*f*	0.13606(7)	0.11370(2)	0.78913(7)	0.0051(1)
Lu3	4*f*	0.62176(8)	0.11902(2)	0.28943(7)	0.0056(1)
Pd1	4*f*	0.07436(13)	0.08476(3)	0.14089(12)	0.0072(1)
Pd2	4*f*	0.42601(13)	0.58211(3)	0.35985(12)	0.0075(1)
Ge1	2*e*	0.0515(2)	1/4	0.28977(15)	0.0081(2)
Ge2	2*e*	0.3343(2)	1/4	0.58221(15)	0.0078(2)
Ge3	2*e*	0.7797(2)	1/4	0.5814(2)	0.0063(2)
Ge4	4*f*	0.15453(17)	0.04252(5)	0.44776(16)	0.0071(1)
Ge5	2*e*	0.2797(2)	1/4	0.0606(2)	0.0048(2)
Ge6	4*f*	0.34622(17)	0.54443(4)	0.05049(16)	0.0060(1)
			$Lu_3Pd_4Ge_4$		
Lu1	2*a*	0	0	0	0.0110(2)
Lu2	4*j*	1/2	0	0.37347(4)	0.0081(2)
Pd	8*l*	0	0.30094(10)	0.32738(5)	0.0155(3)
Ge1	4*h*	0	0.18745(17)	1/2	0.0084(3)
Ge2	4*i*	0	0	0.21754(10)	0.0132(3)

Similar to $(Tm/Er)_5Pd_4Ge_8$ [4], the presence of Ge covalent fragments in $Lu_5Pd_4Ge_8$ is obvious. Among these, there were two almost identical Ge–Ge dumbbells distanced at 2.49 Å and one more finite fragment composed of four germanium atoms having a *cis*-configuration (Figure 2, Table 4). The latter manifests a small geometrical distortion from the ideal conformation due to slightly different chemical arrangements around terminal Ge atoms (terminal atoms are located at 2.56 and 2.63 Å far from central dumbbell; the internal obtuse angles are ca. 111° and 113°, respectively). The *cis* unit is planar and lays at the mirror plane of the $P2_1/m$ space group. The cited covalent fragments are joined together through Pd–Ge contacts shortened with respect to metallic radii sum (ranging from 2.51 to 2.73 Å) in a complex network hosting Lu atoms in the biggest cavities (see Figure 2). The shortest Lu–Pd and Lu–Ge contacts do not manifest noticeable deviations from the expected values and are ca. 3.0 Å.

Table 4. Interatomic distances and integrated crystal orbital Hamilton populations (-*i*COHP, eV/cell) at E_F for the strongest contacts within the first coordination spheres in $Lu_5Pd_4Ge_8$. Symbols (2*b*) and (1*b*) indicate the number of homocontacts for corresponding Ge species.

Central Atom	Adjacent Atoms	*d* (Å)	-*i*COHP	Central Atom	Adjacent Atoms	*d* (Å)	-*i*COHP	Central Atom	Adjacent Atoms	*d* (Å)	-*i*COHP
Lu1	Ge6 (×2)	2.853	1.26	Lu3	Ge5	2.904	1.25	(1*b*)Ge6	Ge6	2.494	2.39
	Ge1	3.025	0.81		Ge3	2.938	1.25		Pd1	2.516	2.16
	Ge5	3.033	1.02		Pd1	3.042	0.71		Pd2	2.533	2.12
	Ge3	3.036	0.85		Ge1	3.051	0.92		Pd1	2.619	1.80
	Ge2	3.064	0.79		Pd2	3.063	0.68		Lu1	2.853	1.26
	Ge5	3.069	0.81		Ge6	3.072	0.90		Lu2	3.016	0.96
	Pd1 (×2)	3.194	0.52		Ge6	3.094	0.75		Lu2	3.050	0.80
	Pd2 (×2)	3.258	0.46		Pd2	3.100	0.63		Lu3	3.072	0.90
Lu2	Ge5	2.857	1.29		Ge4	3.105	0.71		Lu3	3.094	0.75
	Ge3	2.918	1.20		Ge4	3.120	0.84	Pd1	Ge6	2.516	2.16
	Ge2	2.994	0.99		Pd1	3.236	0.52		Ge4	2.526	2.11
	Ge6	3.016	0.95		Ge4	3.493	0.27		Ge1	2.606	1.66
	Ge4	3.043	0.91	(1*b*)Ge3	Ge2	2.559	1.92		Ge6	2.619	1.80
	Ge4	3.043	0.79		Pd2 (×2)	2.699	1.46		Ge5	2.730	1.35
	Ge6	3.050	0.80		Lu2 (×2)	2.918	1.20		Lu3	3.042	0.71
	Pd1	3.087	0.68		Lu3 (×2)	2.938	1.25		Lu2	3.087	0.68
	Pd1	3.104	0.63		Lu1	3.036	0.86		Lu2	3.104	0.63
	Pd2	3.114	0.64	(1*b*)Ge4	Ge4	2.492	2.48		Lu1	3.194	0.52
	Pd2	3.156	0.57		Pd2	2.512	2.14	Pd2	Ge4	2.512	2.14
(2*b*)Ge1	Ge2	2.484	2.98		Pd1	2.526	2.11		Ge6	2.533	2.12
	Pd1 (×2)	2.606	1.66		Pd2	2.566	1.94		Ge4	2.566	1.94
	Ge5	2.627	1.69		Lu2	3.043	0.91		Ge2	2.649	1.53
	Lu1	3.025	0.81		Lu2	3.043	0.79		Ge3	2.699	1.46
	Lu3 (×2)	3.051	0.92		Lu3	3.105	0.71		Lu3	3.063	0.68
(2*b*)Ge2	Ge1	2.484	2.98	(1*b*)Ge5	Ge1	2.627	1.69		Lu3	3.100	0.63
	Ge3	2.559	1.92		Pd1 (×2)	2.730	1.35		Lu2	3.114	0.65
	Pd2 (×2)	2.649	1.53		Lu2 (×2)	2.857	1.29		Lu2	3.156	0.58
	Lu2 (×2)	2.994	1.00		Lu3 (×2)	2.904	1.26				
	Lu1	3.064	0.79		Lu1	3.033	1.02				
					Lu1	3.069	0.81				

The $Lu_3Pd_4Ge_4$ contains less germanium with respect to $Lu_5Pd_4Ge_8$ and, consequently, only a simple Ge–Ge dumbbell forms being, however, more stretched (2.59 Å, Table 5). The trend of other interactions is similar as for $Lu_5Pd_4Ge_8$; Pd and Ge construct an extended network with infinite channels of hexagonal and pentagonal forms hosting Lu atoms.

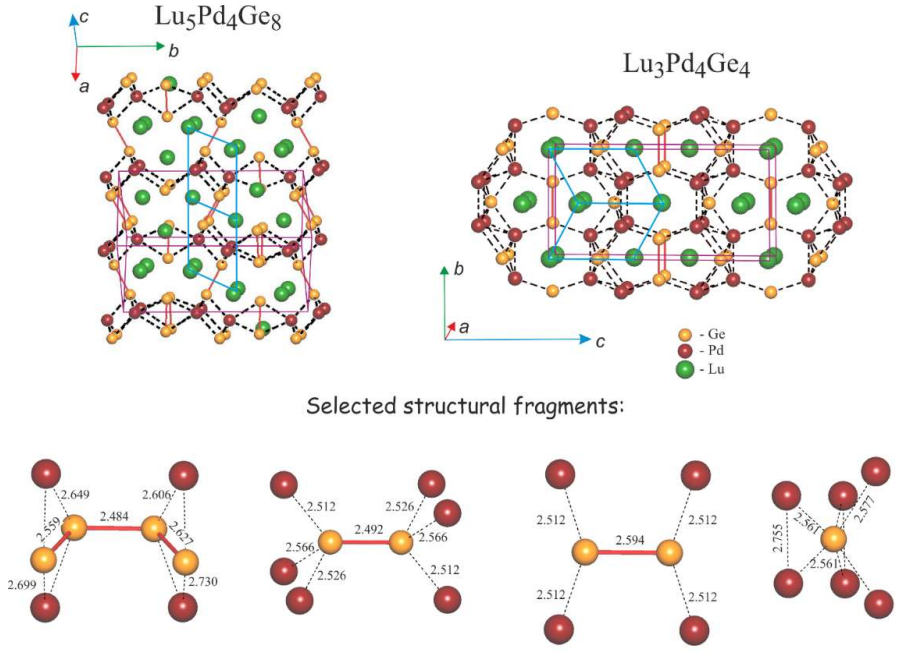

Figure 2. Crystal structures of $Lu_5Pd_4Ge_8$ and $Lu_3Pd_4Ge_4$. The Pd–Ge frameworks are evidenced by dotted lines. Ge–Ge covalent bonds are shown by red sticks. Selected fragments, discussed in the text, are pictured at the bottom. Selected interatomic distances (Å) are indicated. $ThCr_2Si_2$-like fragments are evidenced in blue.

Table 5. Interatomic distances and integrated crystal orbital Hamilton populations (-*i*COHP, eV/cell) at E_F for the strongest contacts within the first coordination spheres in $Lu_3Pd_4Ge_4$. Symbols (1*b*) and (0*b*) indicate the number of homocontacts for corresponding Ge species.

Central Atom	Adjacent Atoms	*d* (Å)	-*i*COHP	Central Atom	Adjacent Atoms	*d* (Å)	-*i*COHP
Lu1	Ge4 (×4)	2.992	1.21	(0*b*)Ge2	Pd (×4)	2.562	1.88
	Ge5 (×2)	3.006	1.05		Pd (×2)	2.577	1.86
	Pd (×8)	3.445	0.41		Lu2 (×2)	2.988	0.83
Lu2	Ge5 (×2)	2.988	0.83		Lu1	3.006	1.05
	Ge4 (×4)	3.003	0.99	Pd	Ge4	2.512	2.23
	Pd (×4)	3.003	0.79		Ge5 (×2)	2.562	1.88
	Pd (×2)	3.100	0.58		Pd	2.755	0.97
(1*b*)Ge1	Pd (×2)	2.512	2.23		Lu2 (×2)	3.003	0.79
	Ge1	2.595	1.82		Pd (×2)	3.058	0.46
	Lu1 (×2)	2.992	1.22		Lu2	3.100	0.58
	Lu2 (×4)	3.003	0.99		Lu1 (×2)	3.445	0.41

One more structural relation can be proposed for the title compounds: both compounds contain common structural $ThCr_2Si_2$-like building blocks [31] (highlighted by blue lines in Figure 2) defined in many related compounds as "linkers" within various polyanionic fragments [32].

3.2.2. $Lu_5Pd_4Ge_8$: Structural Relationships

Looking for structural relationships is not an easy task, since this process is often strongly affected by human factors and is based on sometimes arbitrary criteria. From this point of view, one of the most rigorous approaches is based on the symmetry principle within the group-subgroup theory [33]. The most frequent chemical reason causing the reduction of symmetry is so-called "coloring", which can be interpreted as an ordered distribution of different chemical elements within distinct Wyckoff sites. Müller [34] and Pöttgen [35] depict numerous examples of these.

Structural relationships between $Tm_5Pd_4Ge_8$ (isostructural with $Lu_5Pd_4Ge_8$) and $RE_3T_2Ge_3$ (T = late transitional element) were proposed in the literature [2] based on topological similarities between polyanionic fragments and the spatial distribution of cations. An alternative description of relationships between the abovementioned structures in terms of symmetry reduction is proposed here. The stoichiometries of these compounds are related as follows:

$$4\ RE_3T_2Ge_3 - 2\ RE + 4\ Ge = 2\ RE_5T_4Ge_8 \quad (1)$$

This relation, even if purely numerical, finds support when comparing the crystal structures of the two chemically affine representatives $Lu_3Fe_2Ge_3$ (*oS*32) and $Lu_5Pd_4Ge_8$ (*mP*34). As is evidenced in Figure 3, one of the Lu sites in the former is substituted by a Ge dumbbell in the latter.

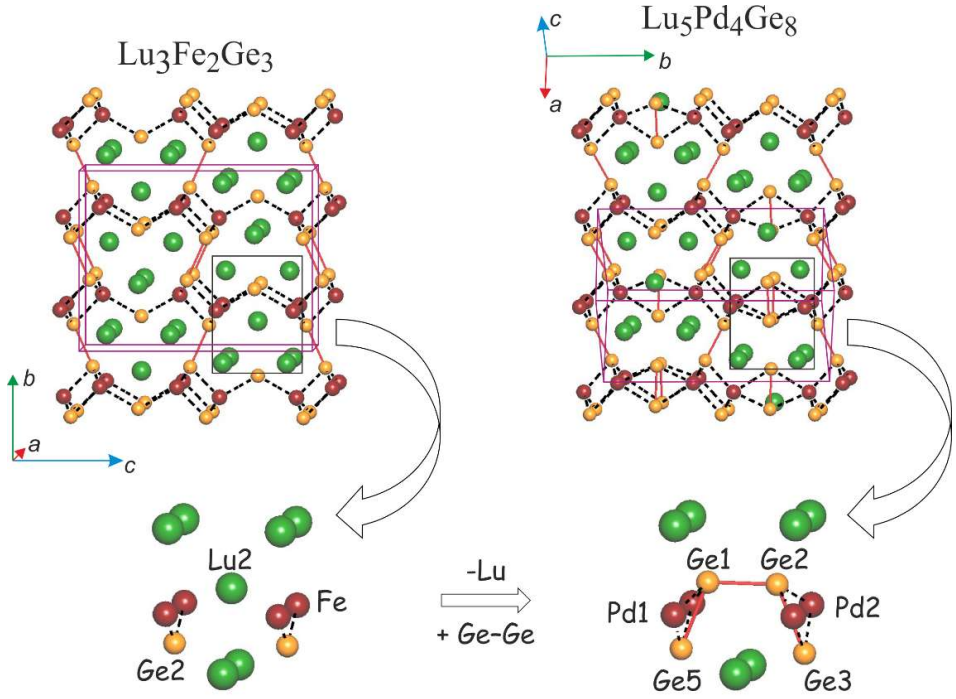

Figure 3. Structural similarities between $Lu_3Fe_2Ge_3$ and $Lu_5Pd_4Ge_8$. The polyanionic networks are shown by dotted lines, and covalent Ge fragments are joined by red sticks. The grey rectangle evidences regions of the crystal space where Lu/Ge_2 substitution takes place (for details see text).

From the chemical interaction point of view, this should be a drastic change; instead, the remaining atoms apparently do not suffer noticeable displacements. This is why it was checked whether a Bärnighausen tree might be constructed relating the *oS*32 and *mP*34 models. In fact, only two reduction steps were needed:

- a *traslationengleiche* (t2) decentering leading to a monoclinic Niggli cell ($mP16$-$P2_1/m$).
- a *klassengleiche* transformation (k2) giving a monoclinic model with doubled cell volume ($mP32$-$P2_1/m$). As a result, all the independent sites split in two (see Figure 4).

The Lu2′ site (2*e*: *0.211* 1/4 *0.430*) was further substituted by two germanium atoms (positions Ge1 and Ge2 in the final *mP*34-$P2_1/m$ structural model). As a result, the already cited *cis*-Ge4 unit forms (see Figure 2), whose chemical role is discussed in the next section. The presence of the *cis*-Ge_4 units is quite intriguing, since the *trans* conformation is more favorable in numerous molecular chemistry examples. Therefore, it was decided to generate a structural model of $Lu_5Pd_4Ge_8$ composition hosting the *trans*-Ge unit and optimize it (see Figure S1 and Table S1). The relaxed structure perfectly coincided with the experimental results, confirming that minimal energy is associated with the *cis* conformation. More details on this, including an animation showing the evolution of the structural model after each relaxation step, are available in the Supplementary Material.

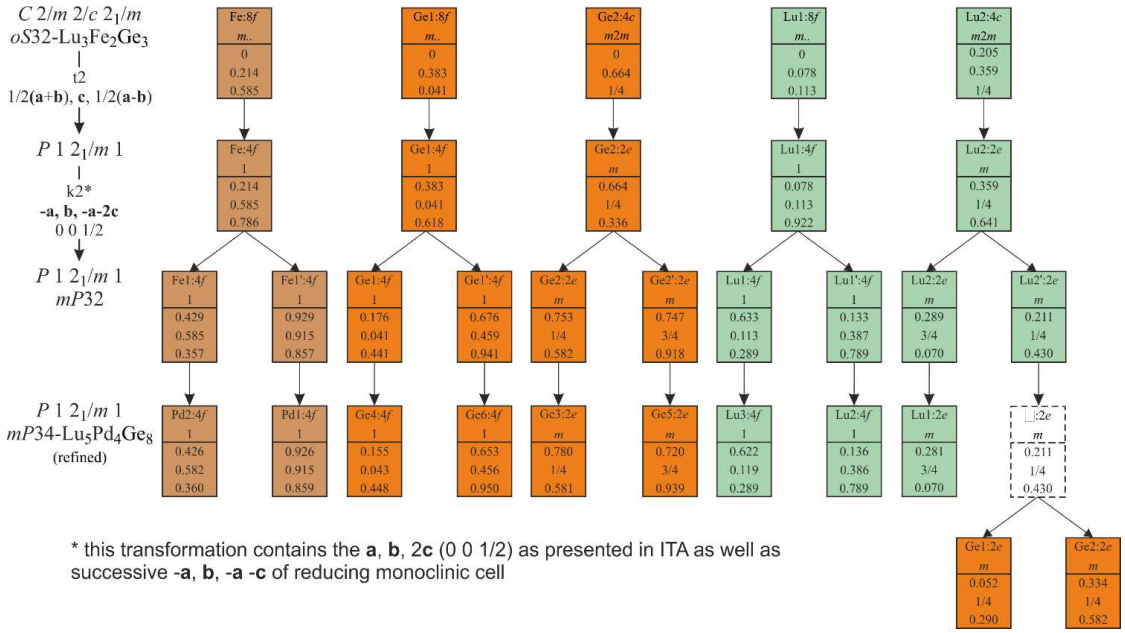

Figure 4. Evolution of the atomic parameters within the Bärnighausen formalism accompanying the symmetry reduction from $Lu_3Fe_2Ge_3$ to $Lu_5Pd_4Ge_8$ structures. The background colors correspond to the atom markers in the figures through the text.

3.3. Chemical Bonding Analysis

Frequently, chemical bonding in polar intermetallics is preliminary addressed using the *Zintl-Klemm* concept. Taking into account the interatomic distances between Ge atoms, the presence of [(1*b*)Ge^{3-}] with [(2*b*)Ge^{2-}] Zintl species in $Lu_5Pd_4Ge_8$ and [(1*b*)Ge^{3-}] with [(0*b*)Ge^{4-}] ones in $Lu_3Pd_4Ge_4$ could be guessed. In order to guarantee the precise electron count, the average number of valence electrons per Ge atom [*VEC*(Ge)] should amount to 6.75 for $Lu_5Pd_4Ge_8$ and to 7.50 for $Lu_3Pd_4Ge_4$. Although it is reasonable to hypothesize a formal charge transfer of 3 valence electrons per Lu atom (Lu^{3+}), as a first approximation, the Pd could be considered as a divalent cation (Pd^{2+}) or a neutral species (Pd^0). However, none of the possible electron distribution formulae listed below are suitable for the studied compounds, giving *VEC*(Ge) values that deviate somewhat from ideal values.

$$Lu_5Pd_4Ge_8\ (Pd^0)\quad VEC(Ge) = 5.875$$

$$Lu_5Pd_4Ge_8\ (Pd^{2+})\quad VEC(Ge) = 6.875$$

$$Lu_3Pd_4Ge_4\ (Pd^0)\quad VEC(Ge) = 6.250$$

$$Lu_3Pd_4Ge_4\ (Pd^{2+})\quad VEC(Ge) = 8.250$$

Even if the obtained *VEC*(Ge) values are closer to 6.75/7.50, in the case of Pd^{2+}, this assumption is not coherent with the valence electrons flow when considering any of the known electronegativity

scales. For example, taking into account the *Pearson* electronegativity values for Pd (4.45 eV) and Ge (4.60 eV) it is clear that a charge transfer from Pd to Ge is hardly probable. Strictly speaking, it is not possible to successfully apply the (8–*N*) rule to interpret the Ge–Ge covalent interactions. Thus, it becomes clear that these simplified considerations are not sufficient to account for the chemical bonding of the studied intermetallics. In particular, it is not reliable to consider covalent Ge fragments as isolated and more complex interactions should be taken into account. Therefore, a deeper chemical bonding investigation was conducted.

In Table 6, the volumes of the atomic basins and Bader effective charges for all the atoms in $Lu_5Pd_4Ge_8$ and $Lu_3Pd_4Ge_4$ are listed together with those for the same species in their pure element form. Comparing these values, one can qualitatively estimate the chemical role of constituents in binary/ternary compounds.

Table 6. Calculated QTAIM effective charges and atomic basin volumes for Lu, Pd and Ge in their elemental structure, in $Lu_5Pd_4Ge_8$ and in $Lu_3Pd_4Ge_4$.

Element/Compound	Atom/Site	Volume, [Å^3]	QTAIM Charge, Q^{eff}	Compound	Atom/Site	Volume, [Å^3]	QTAIM Charge, Q^{eff}
Lu (*hP*2)	Lu/2*c*	29.74 #	0	$Lu_5Pd_4Ge_8$	Lu1/2*e*	15.88	+1.45
Pd (*cF*4)	Pd/4*a*	14.71 #	0	(*mP*34)	Lu2/4*f*	15.48	+1.48
Ge (*cF*8)	Ge/8*a*	22.66 #	0		Lu3/4*f*	15.85	+1.51
					Pd1/4*f*	19.91	−0.79
$Lu_3Pd_4Ge_4$	Lu1/2*a*	16.90	+1.57		Pd2/4*f*	19.77	−0.76
(*oI*22)	Lu2/4*j*	15.05	+1.53		(2*b*)Ge1/2*e*	19.39	−0.23
	Pd/8*l*	19.43	−0.67		(2*b*)Ge2/2*e*	19.51	−0.30
	(1*b*)Ge1/4*h*	22.35	−0.89		(1*b*)Ge3/2e	22.66	−0.87
	(0*b*)Ge2/4*i*	16.42	−0.09		(1*b*)Ge4/4*f*	18.73	−0.30
					(1*b*)Ge5/2*e*	23.96	−1.14
					(1*b*)Ge6/4*f*	19.67	−0.59

#—the QTAIM volumes of atoms in pure elements are equal to the volumes of their Wigner–Seitz polyhedra; structural data were taken from Ref [1].

In both ternary germanides, the QTAIM basins of Lu were shrunk with respect to Lu-*hP*2, and the corresponding charges oscillated around +1.5, confirming the active metal-like role of Lu. The significant difference between Lu effective charges and the formal charges suggest that some of its valence electrons may contribute to covalent interactions.

The palladium atoms had similar volumes of atomic basins (ca. 20 Å^3) and are negatively charged ($-0.7 \div -0.8$), suggesting a bonding scenario coherent with the electronegativity values, i.e., with Pd taking part in a polyanionic network, as was hypothesized from the crystal structure analysis.

It is noteworthy that in the same compound, Ge atoms had pronounced differences in charge values (always negative) from site to site. More on the structural/chemical reasons for this will be discussed in the following.

The total and projected DOS for Lu, Pd and Ge for the studied intermetallics are shown in Figure 5. Orbital projected DOS can be found in the Supplementary Material (Figure S3). Focusing on the total DOS, a difference between the two compounds at the Fermi energy (E_F) is evident: for $Lu_5Pd_4Ge_8$ a pseudo-gap is visible just above E_F, instead for $Lu_3Pd_4Ge_4$ the Fermi level corresponds to a local maximum of the DOS, indicating a potential electronic instability. This might be a sign of particular physical properties (e.g., superconductivity or magnetic ordering) [36] or of small structural adjustments (e.g., off-stoichiometry due to statistical mixture or increase of vacancy concentration) [37] which, adequately modelled, would shift the E_F towards a local minimum. Even if EDXS elementary composition is compatible with a slightly off-stoichiometry, there is no strong indication of this coming from XRD data, so, the stoichiometric model was considered here. Further experimental investigations will be carried out aiming physical properties studies of this compound.

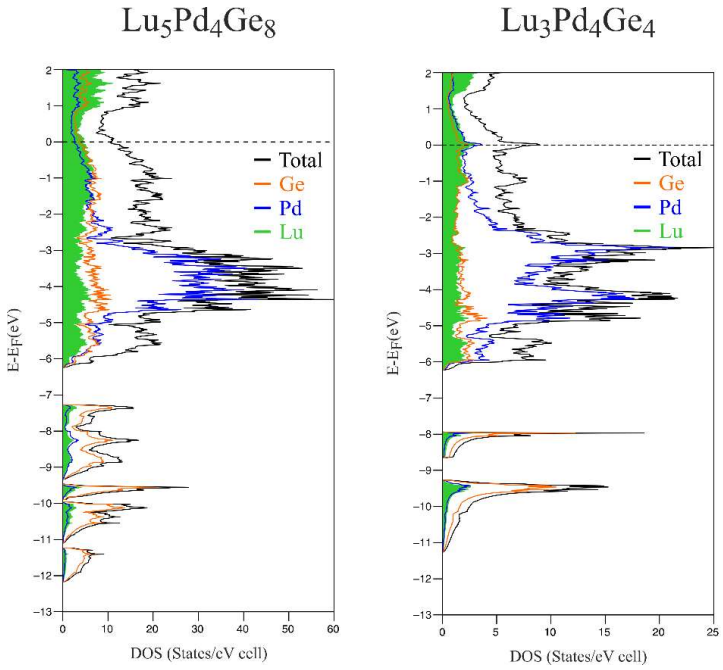

Figure 5. Total and projected DOS for the two studied compounds.

For both compounds, the valence orbital mixing of the three components over the whole energy range is noteworthy. Below E_F, both DOSs showed a gap of around −7 eV separating the two regions, with the lowest being mostly dominated by the *4s* Ge states. The Pd-*d* states are mainly distributed in the range between −5 and −2.5 eV. Their width and energy overlapped with *4p* Ge and Lu states, supporting the bonding relevance of Pd–Ge and Pd–Lu interactions. The fact that the majority of Pd *4d* states are located well below the E_F indicates the electron acceptor character of this species. A significant contribution of *5d* Lu states just below the E_F is a common feature of cations in polar intermetallics, characterized by an incomplete charge transfer (confirmed here also by Bader charge values).

Although the *Zintl–Klemm* (8–*N*) rule cannot be applied for the title compounds, it was decided to trace interaction similarities comparing the electronic structures of ideal Zintl anions Ge_2^{6-} and *cis*-Ge_4^{10-} coming from the extended Hückel calculation with those obtained by means of TB-LMTO-ASA, in terms of COHP curves. Molecular orbital diagrams (MO) for Ge_2^{6-} (point group $D_{\infty h}$) and Ge_4^{10-} (the point symmetry of this anion was forced to C_{2v} fixing for all distances to 2.56 Å and obtuse internal angles to 111°) are presented in the Supplementary Materials (Figure S2) with the accordingly labeled orbitals.

In Figure 6a, the molecular orbital overlap population (MOOP) for Ge_2^{6-} is shown, together with COHP curves for Ge–Ge interactions (in dumbbells) existing in $Lu_3Pd_4Ge_4$ and $Lu_5Pd_4Ge_8$.

These partitioning methods could not be directly compared, since MOOP partitions the electron number, instead, COHP partitions the band structure energy. Since they both permit to easily distinguish between bonding and antibonding states, it was decided to perform a qualitative comparison targeting to figure out the similarities/differences between the isolated molecular fragments analogous with those found in the studied compounds.

The presence of the gap (at ca. −7eV) may be attributed to the energy separation of the σ*ss* and σ**ss* of Ge_2 dumbbells from the σ*p*, π*p* and π* orbitals. For the $Lu_3Pd_4Ge_4$ there are some occupied π* states close to E_F, whereas in $Lu_5Pd_4Ge_8$, the cited interactions are almost optimized at E_F. From these observations it derives that Ge dumbbells are not completely polarized; for $Lu_5Pd_4Ge_8$ the dispersion of σ and σ* states is more pronounced. One of the possible explanation of this is the existence of additional covalent interactions between germanium dumbbells and neighboring atoms.

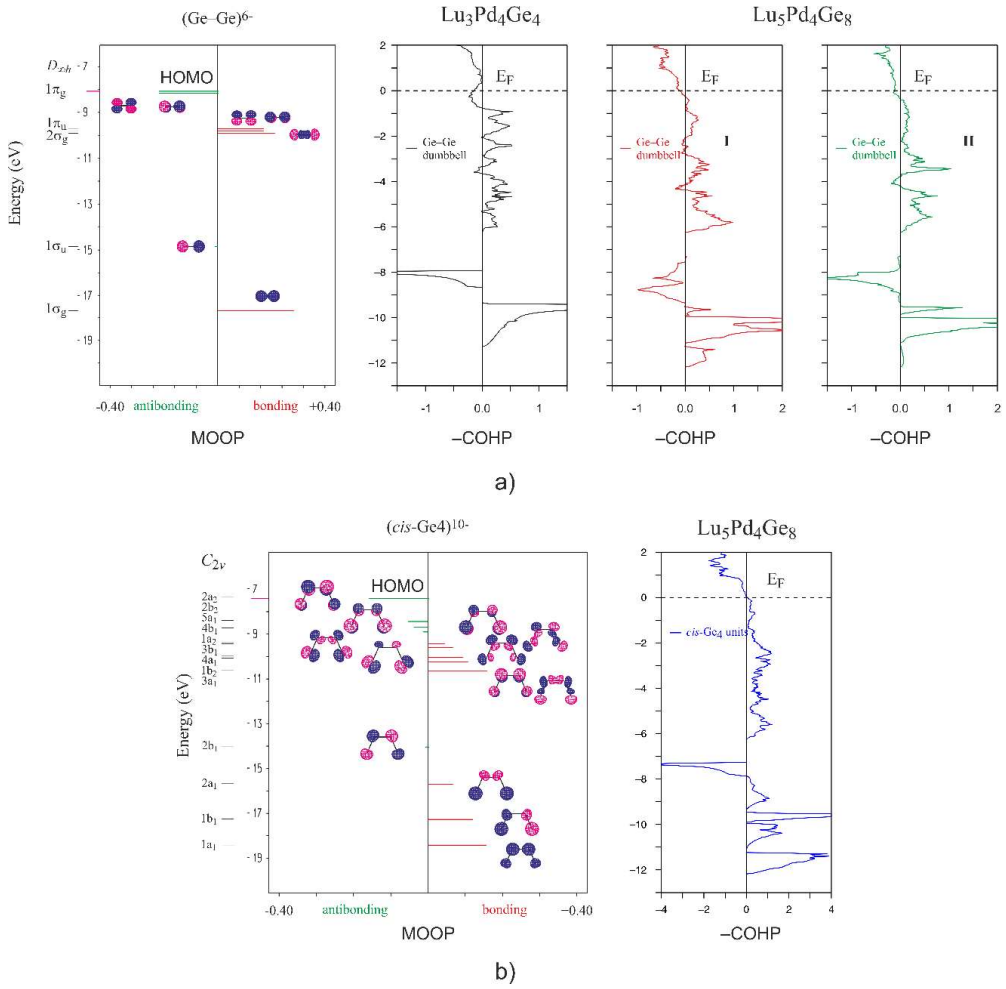

Figure 6. Extended Hückel calculated Molecular Orbital Overlap Population (MOOP) plot for the Ge_2^{6-} (**a**) and *cis*-Ge_4^{10-} (**b**) anions together with the corresponding Crystal Orbital Hamilton Population (COHP) for $Lu_3Pd_4Ge_4$ and $Lu_5Pd_4Ge_8$ (**I** and **II** corresponds to two distinct dumbbells). The degeneracy of the π levels for Ge_2^{6-} is removed for the sake of clarity. The HOMO energy is set in correspondence to E_F.

From the structural data it is known that in $Lu_3Pd_4Ge_4$, Ge atoms are distanced at 2.59 Å as in diverse metal-like salts studied before [38–40]. Instead, in $Lu_5Pd_4Ge_8$ this distance is shortened to 2.49 Å. Usually, the trend of Ge–Ge dumbbell distances is related with electrostatic repulsion between atoms. This statement is coherent with integrated COHP values (–*i*COHP, see Tables 4 and 5) that reflect the same trend, being of −1.82 eV/cell for $Lu_3Pd_4Ge_4$ and of −2.39 and −2.48 eV/cell for $Lu_5Pd_4Ge_8$.

Within the *cis*-Ge_4^{10-} anion the number of covalent interactions is higher, as a result the energy dispersion of its molecular states increases. For example, in the range $-18 \div -14$eV there are four MOs instead of two MOs for dumbbells. A very similar trend/type of interactions derives from COHP curves for $Lu_5Pd_4Ge_8$. As for the dumbbells, the interactions for the *cis* fragment are optimized at the E_F confirming its partial polarization.

Based on –*i*COHP values listed in Tables 4 and 5 it derives that Pd–Ge interactions are very relevant, so one may assume the covalent type of bonding between them. The –COHP plots in Figure 7 confirm that they are mainly of bonding type over a large range below E_F with a weak unfavorable antibonding interaction in the vicinity of E_F, probably due to electrostatic repulsion between Ge orbitals and filled *d* states of Pd.

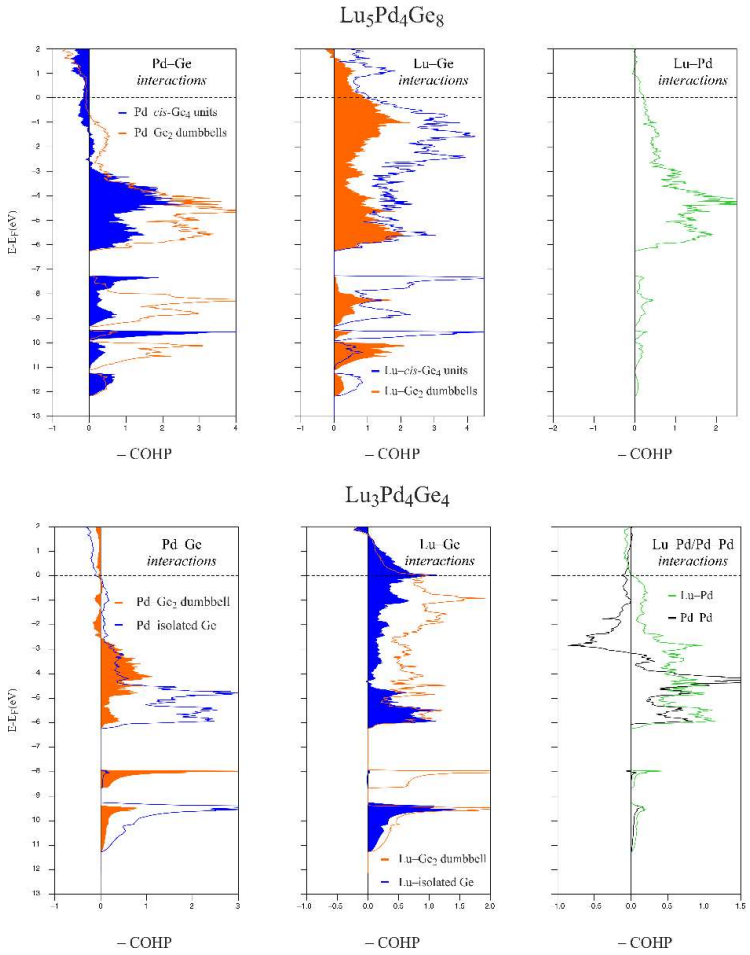

Figure 7. Crystal Orbital Hamilton Populations (–COHP) for selected interactions for the two studied compounds.

Inside $Lu_3Pd_4Ge_4$ the presence of a Pd–Pd short interaction can be highlighted. The –COHP plots for this are similar to those reported for Ca_2Pd_3Ge [41] showing a sharp antibonding character around −3 eV commonly attributed to enhanced repulsion between filled *d* states of Pd. Nevertheless, they are of bonding type in average as deducible from the –*i*COHP values for this interaction (0.97 eV/cell), comparable to those reported in [41].

The remaining Lu–Pd and Ge–Lu interactions are weaker being however very similar for both germanides. All of them are of bonding type, Lu–Pd interactions are practically optimized at Fermi level. Numerous interactions between Lu and Pd (Lu and Ge) suggest that some covalent-like interaction may exist due to mixing between *d* states of Lu and Pd (or *d* states of Lu with *p* of Ge; similarly, as it was reported for Ca_5Ge_3 [36] and CaSi [42]). More detailed studies are needed in order to interpret these interactions.

The existence of the complex Pd–Ge polyanion (illustrated in Figure 2) and the electronegativity difference between Pd and Ge explains the trend of Ge species charges (listed in Table 6). The Ge dumbbell in $Lu_3Pd_4Ge_4$ has four neighboring Pd atoms, instead those in $Lu_5Pd_4Ge_8$ install six Pd–Ge polar interactions. As a result, the latter Ge species has lower negative charges. The same is true for (0b)Ge atom with six palladium atoms around in $Lu_3Pd_4Ge_4$: its charge approaches to zero. Within crystal structure, the number of Pd–Ge contacts is the same for terminal and central atoms of *cis*–Ge_4 units; thus, their charges trend is similar as for ideal *cis*-Ge_4^{10-} anion, terminal atoms being more negative.

4. Conclusions

The two new $Lu_5Pd_4Ge_8$ and $Lu_3Pd_4Ge_4$ polar intermetallics were synthesized and characterized in this work. They were found to crystallize in the *mP*34–$Tm_5Pd_4Ge_8$ and *oI*22–$Gd_3Cu_4Ge_4$ structures respectively. A detailed description of crystal structure solution in the case of the non-merohedral twinned crystal of $Lu_5Pd_4Ge_8$ was proposed, highlighting the difficulties/problems encountered here along with practical suggestions to manage them.

Joined crystal chemical analysis and combined DFT studies suggest the presence of $[Pd_4Ge_8]^{7.4-}$ and $[Pd_4Ge_4]^{4.6-}$ polyanions. The interactions of Lu with these frameworks cannot be viewed as purely ionic as derives from its states distribution, COHP analysis and Bader charges. The Lu–Pd and Lu–Ge bonding interactions are one of the most interesting aspects arisen from our study and their nature deserves further investigations.

Supplementary Materials: The following are available online at http://www.mdpi.com/2073-4352/8/5/205/s1, Figure S1: Schematic representation of the structural relationships between "cis" and "trans" Ge_4 fragments in $Lu_5Pd_4Ge_8$ models; Figure S2: Molecular orbitals diagram for Ge_2^{6-} (a) and *cis*-Ge_4^{10-} (b) as generated by CACAO; Figure S3: Total DOS for $Lu_5Pd_4Ge_8$ and $Lu_3Pd_4Ge_4$ together with the orbital projected DOS for each species; Table S1: Atomic parameters for "trans"-$Lu_5Pd_4Ge_8$ model. Video S1: $Lu_5Pd_4Ge_8$_trans-cis_optimization, $Lu_5Pd_4Ge_8$ CIF file, $Lu_3Pd_4Ge_4$ CIF file.

Author Contributions: Riccardo Freccero, Pavlo Solokha and Serena De Negri conceived and designed the experiments; Riccardo Freccero performed the syntheses; Pavlo Solokha and Davide Maria Proserpio performed the XRD single crystal experiments; Serena De Negri performed SEM analyses; Riccardo Freccero, Pavlo Solokha and Davide Maria Proserpio conducted different calculations; Riccardo Freccero, Pavlo Solokha, Serena De Negri and Adriana Saccone analyzed the data and wrote the paper.

Acknowledgments: The authors thank Roman Eremin from SCTMS (Samara State University, Russia) for his contribution in the Bader charge analysis.

Conflicts of Interest: The authors declare no conflict of interest.

References

1. Villars, P.; Cenzual, K. *Pearson's Crystal Data*; ASM International: Metals Park, OH, USA, 2018.
2. Freccero, R.; Solokha, P.; Proserpio, D.M.; Saccone, A.; De Negri, S. A new glance on R_2MGe_6 (R = rare earth metal, M = another metal) compounds. An experimental and theoretical study of R_2PdGe_6 germanides. *Dalton Trans.* **2017**, *46*, 14021–14033. [CrossRef] [PubMed]
3. Niepman, D.; Prots, Y.M.; Pöttgen, R.; Jeitschko, W. The order of the palladium and germanium atoms in the germanides *Ln*PdGe (*Ln* = La–Nd, Sm, Gd, Tb) and the new compound $Yb_3Pd_4Ge_4$. *J. Solid State Chem.* **2000**, *154*, 329–337. [CrossRef]
4. Heying, B.; Rodewald, U.C.; Pöttgen, R. The germanides $Er_5Pd_4Ge_8$ and $Tm_5Pd_4Ge_8$—3D $[Pd_4Ge_8]$ polyanions with Ge_2 dumb-bells and Ge_4 chains in *cis*-conformation. *Z. Kristallogr.* **2017**, *232*, 435–440. [CrossRef]
5. Feyerherm, R.; Becker, B.; Collins, M.F.; Mydosh, J.; Nieuwenhuys, G.J.; Ramakrishnan, S. The magnetic structure of $CePd_2Ge_2$ and $Ce_2Pd_3Ge_5$. *Phys. B* **1998**, *241–243*, 643–645. [CrossRef]
6. Anand, V.K.; Thamizhavel, A.; Ramakrishnan, S.; Hossain, Z. Complex magnetic order in $Pr_2Pd_3Ge_5$: A single crystal study. *J. Phys.* **2012**, *24*. [CrossRef] [PubMed]
7. Solokha, P.; Freccero, R.; De Negri, S.; Proserpio, D.M.; Saccone, A. The $R_2Pd_3Ge_5$ (R = La–Nd, Sm) germanides: Synthesis, crystal structure and symmetry reduction. *Struct. Chem.* **2016**, *27*, 1693–1701. [CrossRef]
8. Rodewald, U.C.; Heying, B.; Hoffmann, R.-D.; Niepmann, D. Polymorphism in the germanides REPdGe with the heavy rare earth elements. *Z. Naturforsch.* **2009**, *64b*, 595–602. [CrossRef]
9. Chabot, B.; Parthé, E. $Dy_2Co_3Si_5$, $Lu_2Co_3Si_5$, $Y_2Co_3Si_5$ and $Sc_2Co_3Si_5$ with a monoclinic structural deformation variant of the orthorhombic $U_2Co_3Si_5$ structure type. *J. Less-Common Met.* **1985**, *106*, 53–59. [CrossRef]
10. Bruker. APEX2, SAINT-Plus, XPREP, SADABS, CELL_NOW and TWINABS. Bruker AXS Inc.: Madison, WI, USA, 2014.
11. Kraus, W.; Nolze, G. POWDER CELL-A program for the representation and manipulation of crystal structure and calculation of the resulting X-ray powder pattern. *J. Appl. Crystallogr.* **1996**, *29*. [CrossRef]

12. Bader, R.F. *Atoms in Molecules: A Quantum Theory*; Clarendon Press and Oxford University Press: New York, NY, USA, 1994.
13. Kresse, G.; Furthmüller, J. Efficient iterative schemes for ab initio total-energy calculations using a plane-wave basis set. *J. Phys. Rev. B* **1996**, *54*, 11169–11186. [CrossRef]
14. Krier, G.; Jepsen, O.; Burkhardt, A.; Andersen, O.K. *The TB-LMTO-ASA Program*; Version 4.7; Max-Planck-Institut Für Festkörperforschung: Stuttgart, Germany, 2000.
15. Barth, U.; Hedin, L.A. Local exchange-correlation potential for the spin polarized case: I. *J. Phys. Chem.* **1972**, *C5*, 1629–1642. [CrossRef]
16. Dronskowski, R.; Blöchl, P.E. Crystal orbital Hamilton populations (COHP): Energy-resolved visualization of chemical bonding in solids based on density-functional calculations. *J. Phys. Chem.* **1993**, *97*, 8617–8624. [CrossRef]
17. Eck, B. Wxdragon, Aachen, Germany, 1994–2018. Available online: http://wxdragon.de/ (accessed on 2 May 2018).
18. Mealli, C.; Proserpio, D.M. MO Theory made visible. *J. Chem. Educ.* **1990**, *67*, 399–403. [CrossRef]
19. Mealli, C.; Ienco, A.; Proserpio, D.M. *Book of Abstracts of the XXXIII. ICCC*; ICCC: Florence, Italy, 1998.
20. Lowe, J.; Peterson, K. *Quantum Chemistry*, 3rd ed.; Academic Press: Cambridge, MA, USA, 2005.
21. Hoffmann, R. *Solids and Surfaces: A Chemist's View of Bonding in Extended Structures*; VCH: New York, NY, USA, 1988.
22. Solokha, P.; De Negri, S.; Saccone, A.; Proserpio, D.M. On a non-merohedrally twinned Tb_3Ge_5 crystal. In Proceedings of the XII International Conference on Crystal Chemistry of Intermetallic Compounds, Lviv, Ukraine, 22–26 September 2012.
23. Budnyk, S.L.; Weitzer, F.; Kubata, C.; Prots, Y.; Akselrud, L.G.; Schnelle, W.; Hiebl, K.; Nesper, R.; Wagner, F.R.; Grin, Yu. Barrelane-like germanium clusters in Eu_3Ge_5: Crystal structure, chemical bonding and physical properties. *J. Solid State Chem.* **2006**, *179*, 2329–2338. [CrossRef]
24. Shcherban, O.; Savysyuk, I.; Semuso, N.; Gladyshevskii, R.; Cenzual, K. Crystal structure of the compound Pr_4Ge_7. *Chem. Met. Alloys* **2009**, *2*, 115–122.
25. Müller, P. *Crystal Structure Refinement: A Crystallographer's Guide to SHELXL*; Oxford University Press: Oxford, UK, 2006.
26. Clegg, W. *Crystal Structure Analysis: Principle and Practice*, 2nd ed.; Oxford University Press: Oxford, UK, 2009.
27. Petricek, V.; Dusek, M.; Palatinus, L. Crystallographic computing system JANA2006: General features. *Z. Kristallogr.* **2014**, *229*, 345–352.
28. Cooper, R.I.; Gould, R.O.; Parsons, S.; Watkin, D.J. The derivation of non-merohedral twin laws during refinement by analysis of poorly fitting intensity data and the refinement of non-merohedrally twinned crystal structures in the program crystals. *J. Appl. Crystallogr.* **2002**, *35*, 168–174. [CrossRef]
29. Farrugia, L.J. WinGX and ORTEP for windows: An update. *J. Appl. Cryst.* **2012**, *45*, 849–854. [CrossRef]
30. Gelato, L.; Parthé, E. *Structure tidy*—A computer program to standardize crystal structure data. *J. Appl. Crystallogr.* **1987**, *20*, 139–143. [CrossRef]
31. Parthé, E.; Gelato, L.; Chabot, B.; Penzo, M.; Cenzual, K.; Gladyshevskii, R. *TYPIX Standardized Data and Crystal Chemical Characterization of Inorganic Structure Types*; Springer-Verlag: Heidelberg, Germany, 1993.
32. Prots, Y.; Demchyna, R.; Burkhardt, U.; Schwarz, U. Crystal structure and twinning of HfPdGe. *Z. Kristallogr.* **2007**, *222*, 513–520. [CrossRef]
33. Wondratschek, H.; Müller, U. *International Tables for Crystallography, Symmetry Relations between Space Groups*; Vol. A1; Kluwer Academic Publishers: Dordrecht, The Netherlands, 2004.
34. Müller, U. *Symmetry Relationships between Crystal Structures. Applications of Crystallographic Group Theory in Crystal Chemistry*; Oxford University Press: Oxford, UK, 2013.
35. Pöttgen, R. Coloring, distortions, and puckering in selected intermetallic structures from the perspective of group—Subgroup relations. *Z. Anorg. Allg. Chem.* **2014**, *640*, 869–891. [CrossRef]
36. Landrum, G.A.; Dronskowski, R. The orbital origins of magnetism: from atoms to molecules to ferromagnetic alloys. *Angew. Chem. Int. Ed.* **2000**, *39*, 1560–1585. [CrossRef]
37. Lin, Q.; Corbett, J.D. Centric and non-centric $Ca_3Au_{\sim 7.5}Ge_{\sim 3.5}$: Electron-poor derivatives of La_3Al_{11}. syntheses, structures, and bonding analyses. *Inorg. Chem.* **2009**, *48*, 5403–5411. [CrossRef] [PubMed]
38. Mudring, A.-V.; Corbett, J.D. Unusual electronic and bonding properties of the zintl phase Ca_5Ge_3 and related compounds. A theoretical analysis. *J. Am. Chem. Soc.* **2004**, *126*, 5277–5281. [CrossRef] [PubMed]

39. Siggelkow, L.; Hlukhyy, V.; Fässler, T.F. Sr_7Ge_6, Ba_7Ge_6 and Ba_3Sn_2—Three new binary compounds containing dumbbells and four-membered chains of tetrel atoms with considerable Ge-Ge π-bonding character. *J. Solid State Chem.* **2012**, *191*, 76–89. [CrossRef]
40. Eisenmann, B.; Schäfer, H. Zur Strukturchemie der Verbindungsreihe $BaMg_2X_2$ (X = Si, Ge, Sn, Pb). *Z. Anorg. Allg. Chem.* **1974**, *403*, 163–172. [CrossRef]
41. Doverbratt, I.; Ponou, S.; Lidin, S. Ca_2Pd_3Ge, a new fully ordered ternary Laves phase structure. *J. Solid State Chem.* **2013**, *197*, 312–316. [CrossRef]
42. Kurylyshyn, I.M.; Fässler, T.F.; Fischer, A.; Hauf, C.; Eickerling, G.; Presnitz, M.; Scherer, W. Probing the Zintl-Klemm concept: A combined experimental and theoretical charge density study of the Zintl phase CaSi. *Angew. Chem. Int. Ed.* **2014**, *53*, 3029–3032. [CrossRef] [PubMed]